

# Optimal training of variational quantum algorithms without barren plateaus

Tobias Haug<sup>1,\*</sup> and M. S. Kim<sup>1</sup>

<sup>1</sup>QOLS, Blackett Laboratory, Imperial College London SW7 2AZ, UK

Variational quantum algorithms (VQAs) promise efficient use of near-term quantum computers. However, training these algorithms often requires an extensive amount of time and suffers from the barren plateau problem where the magnitude of the gradients vanishes with increasing number of qubits. Here, we show how to optimally train a VQA for learning quantum states. Parameterized quantum circuits can form Gaussian kernels, which we use to derive optimal adaptive learning rates for gradient ascent. We introduce the generalized quantum natural gradient that features stability and optimized movement in parameter space. Both methods together outperform other optimization routines and can enhance VQAs as well as quantum control techniques. The gradients of the VQA do not vanish when the fidelity between the initial state and the state to be learned is bounded from below. We identify a VQA for quantum simulation with such a constraint that can be trained free of barren plateaus. Finally, we propose the application of Gaussian kernels for quantum machine learning.

Quantum computers promise to tackle important problems that can be difficult for classical computers. To effectively use quantum computers available in the near future [1, 2] variational quantum algorithms (VQAs) have been put forward. These VQAs solve tasks by iteratively updating a parameterized quantum circuit (PQC) with a classical optimization routine in a feedback loop [3–6]. However, training of such VQAs can take an extensive amount of iterations, yielding a long time until the algorithm converges. Further, VQAs are often impeded by the barren plateau problem where the variance of the gradients vanish exponentially with increasing number of qubits [7], specific cost functions [8], entanglement [9] and noise [10]. Further, the optimization routine of VQAs was shown to be NP-hard even for problems that are easy for classical computers [11]. Quantum algorithms that can avoid training PQCs to circumvent the barren plateau problem have been proposed [12–17]. To improve training of VQAs, one can use quantum geometric information via the quantum natural gradient (QNG) [18–20]. However the QNG can be unstable [21] and suffers from barren plateaus as well [22]. With these challenges in mind, an important task for quantum computers is learning quantum states. Here, the PQC is trained to represent a given quantum state. Besides the importance for state preparation, this core routine is encountered in many VQAs, such as the projected variational quantum dynamics method [23, 24], variational fast forwarding [25], learning of scramblers [26], quantum circuit born machines [27], quantum autoencoders [28] and excited state calculations [29].

Here, we show how to optimally train a VQA to represent quantum states. We find that the fidelity between two states forms an approximate Gaussian kernel in respect to the distance in parameter space of the PQC, with the quantum Fisher information metric (QFIM) as the weight matrix. With this result, we derive the optimal adaptive learning rate for gradient ascent. Further, we propose a stable variant of the QNG, the generalized

quantum natural gradient (GQNG). For learning quantum states with a PQC, both methods together outperform other optimization techniques. We analytically derive the variance of the gradient. Under the condition that the fidelity between the initial state and the state to be learned has a lower bound, the variance of the gradient has a lower bound that is independent of the number of qubits. We show a type of VQA, the projected variational quantum dynamics method or restarted quantum dynamics method [23, 24], that can fulfill this condition and thus can be trained free of barren plateaus. Our methods can improve various VQAs and numerical quantum control techniques, and promise implementation on near-term quantum computers. As further application, our results are directly relevant for quantum machine learning. The Gaussian kernel can be realized by hardware-efficient PQCs to run quantum machine learning algorithms on the current quantum hardware.

*Model*— A unitary  $U(\boldsymbol{\theta})$  parameterized by the  $M$ -dimensional parameter vector  $\boldsymbol{\theta} \in \mathbb{R}^M$  generates the quantum state  $|\psi(\boldsymbol{\theta})\rangle = U(\boldsymbol{\theta})|0\rangle$  consisting of  $N$  qubits (see Fig.1a). Our goal is to learn the target parameters  $\boldsymbol{\theta}_t$  that approximate a given target state  $|\psi_t\rangle$  (see Fig.1b). This is achieved by the optimization task  $\boldsymbol{\theta}_t = \text{argmax}_{\boldsymbol{\theta}} K_t(\boldsymbol{\theta})$ , where  $K_t(\boldsymbol{\theta}) = |\langle\psi_t|\psi(\boldsymbol{\theta})\rangle|^2$  is the fidelity. A common approach to optimize the fidelity is standard gradient ascent. Here, one calculates the gradient of the fidelity  $\nabla K_t(\boldsymbol{\theta})$ , which tells us in which direction the fidelity shows the largest increase. Then, the parameter  $\boldsymbol{\theta}$  is iteratively updated with the rule  $\boldsymbol{\theta}' = \boldsymbol{\theta} + \alpha \nabla K_t(\boldsymbol{\theta})$ , where  $\alpha$  is the learning rate. After a number of iterations, the quality of the found approximate solution  $\boldsymbol{\theta}'_t$  is measured with the infidelity

$$\Delta K_t(\boldsymbol{\theta}'_t) = 1 - K_t(\boldsymbol{\theta}'_t) = 1 - |\langle\psi_t|\psi(\boldsymbol{\theta}'_t)\rangle|^2. \quad (1)$$

Two common challenges plague this method. First, the update rule assumes that the parameter space is euclidean, i.e. the fidelity varies at the same rate for every parameter direction. However, in general this is not the

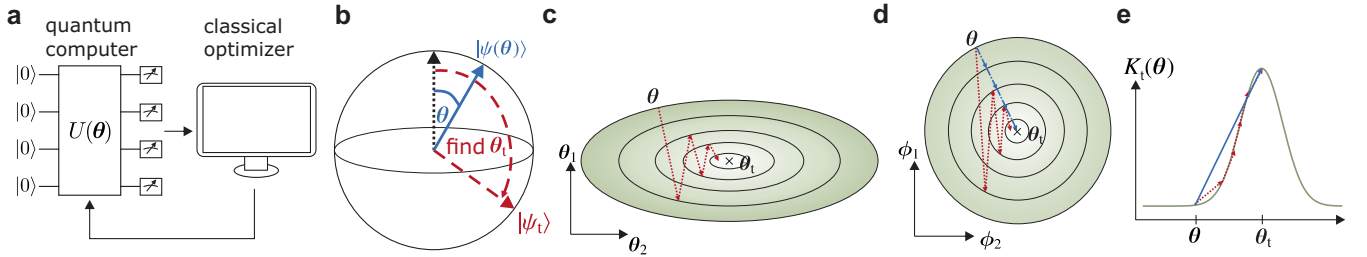


FIG. 1. **a)** The variational quantum algorithm (VQA) consists of a parameterized quantum circuit (PQC) that generates the quantum state  $|\psi(\theta)\rangle = U(\theta)|0\rangle$  with unitary  $U(\theta)$  and parameters  $\theta$ , as well as a classical optimization routine. Measurements on the quantum state are used to calculate the cost function, which is then optimized by the classical optimizer in a feed back loop by adjusting the parameters  $\theta$ . **b)** VQA to represent the target state  $|\psi_t\rangle$  using  $|\psi(\theta)\rangle$ . Goal is to find target parameters  $\theta_t = \operatorname{argmax}_{\theta} K_t(\theta)$  that approximate the target state by maximizing the fidelity  $K_t(\theta) = |\langle\psi_t|\psi(\theta)\rangle|^2$ . **c)** Gradient ascent optimises the fidelity by updating  $\theta' = \theta + \alpha G_0(\theta)$  using the standard gradient  $G_0(\theta) = \nabla K_t(\theta)$ , which points in the direction of steepest increase of fidelity. As the fidelity landscape as function of  $\theta$  is in general not euclidean, standard gradient ascent does not take the fastest path. **d)** By using quantum geometric information about the parameter space with the quantum Fisher information metric (QFIM)  $\mathcal{F}(\theta)$ , the parameter space can be transformed to get the quantum natural gradient (QNG) which moves in the optimal direction (see solid blue curve). However, in practice the QNG is often unstable, which can be solved by a partial transformation which yields the generalized quantum natural gradient (GQNG) (Eq. (5)). **e)** The step size  $\alpha$  for the gradient update is normally a fixed heuristic learning rate (dashed red curve). The fidelity of PQCs can form a Gaussian kernel, which is used to calculate the optimal adaptive learning rate (Eq. (8)) for each gradient update (blue solid curve).

case as seen in Fig. 1c. Then, the standard gradient is not the optimal direction for the parameter update. This can be aided by using the QFIM  $\mathcal{F}(\theta)$ . For  $|\psi\rangle = |\psi(\theta)\rangle$ , it is given by

$$\mathcal{F}_{ij}(\theta) = 4[\langle\partial_i\psi|\partial_j\psi\rangle - \langle\partial_i\psi|\psi\rangle\langle\psi|\partial_j\psi\rangle], \quad (2)$$

where  $\partial_j|\psi\rangle$  is the gradient in respect to the  $j$ -th element of  $\theta$ . For pure states, the QFIM tells us the change of fidelity for small parameter variations  $d\mu$  [22, 30, 31]

$$\mathcal{K}(\theta, \theta + d\mu) = |\langle\psi(\theta)|\psi(\theta + d\mu)\rangle|^2 = 1 - \frac{1}{4}d\mu^T \mathcal{F}(\theta) d\mu. \quad (3)$$

The QFIM contains information about how the geometry of the parameter space is related to the geometry of quantum states. The QNG  $G_1(\theta) = \mathcal{F}^{-1}(\theta)\nabla K_t(\theta)$  [18–20] utilizes this information to construct gradient updates which move optimally in the parameter space (see Fig. 1d). However, when applied in practice the QNG can be unstable [21, 32], which hinders convergence. The second issue is that the learning rate  $\alpha$  is generally not known and has to be determined heuristically, normally by setting it to a small constant. However, by using knowledge about the functional shape of the fidelity as function of  $\theta$ , it is possible to find the optimal learning rate  $\alpha_t$ , which adaptively changes at every step (see Fig. 1e). In the following, we show how to optimally perform gradient ascent to maximize the fidelity by using the GQNG and optimal adaptive learning rates.

We now propose that the fidelity as a function of parameter  $\theta$  can be approximated as a Gaussian kernel. In particular, we have two quantum states of the PQC  $|\psi(\theta)\rangle$  and  $|\psi(\theta')\rangle$  with parameters  $\theta, \theta'$  and a distance

in parameter space  $\Delta\theta = \theta - \theta'$ . Then, the fidelity is given by

$$\mathcal{K}(\theta, \theta') = |\langle\psi(\theta)|\psi(\theta')\rangle|^2 \approx \exp[-\frac{1}{4}\Delta\theta^T \mathcal{F}(\theta) \Delta\theta], \quad (4)$$

where this approximation is valid within a distance  $|\Delta\theta| < \epsilon_G$  with  $\epsilon_G > 0$ . Here, the QFIM  $\mathcal{F}(\theta)$  plays the role of the weight matrix of the kernel. The first order approximation  $\mathcal{K}(\theta, \theta') \approx 1 - \frac{1}{4}\Delta\theta^T \mathcal{F}(\theta) \Delta\theta$  returns Eq. (3) as expected [30, 31]. We show an exactly solvable PQC with Gaussian kernel in the Supplemental Materials. In Fig. 2a, we find that various types of expressive PQCs match well with the Gaussian kernel, which improves with increasing number of qubits. We note that for large parameter norm  $\Delta\theta^T \mathcal{F}(\theta) \Delta\theta$  the fidelity deviates from Eq. (4) and eventually reaches the constant value  $\langle\mathcal{K}_{\text{rand}}\rangle = \frac{1}{2^N}$  given by effectively random states [7, 33]. We can use this result to derive an upper bound for  $\epsilon_G$ . Assuming a simple QFIM  $\mathcal{F} = \frac{I}{b}$  with  $I$  being the identity and  $b > 0$  some constant, we find  $\epsilon_G < 2\sqrt{bN \log(2)}$ .

We now propose to replace the standard gradient  $\nabla K_t(\theta)$  in gradient ascent with the GQNG

$$G_\beta(\theta) = \mathcal{F}^{-\beta}(\theta)\nabla K_t(\theta), \quad (5)$$

where  $\beta \in [0, 1]$ . As special cases, we have the standard gradient for  $G_0(\theta) = \nabla K_t(\theta)$  and the QNG for  $G_1(\theta) = \mathcal{F}^{-1}(\theta)\nabla K_t(\theta)$  [18, 20]. The source of the instability of the QNG is the inverse of the QFIM  $\mathcal{F}^{-1}(\theta)$ , which is highly sensitive to small changes in parameter  $\theta$  when  $\mathcal{F}(\theta)$  is ill conditioned. Regularization of  $\mathcal{F}(\theta)$  was proposed as a way to stabilize the QNG, but that requires

a carefully tuned hyperparameter [21, 32]. The GQNG can overcome this problem in general by tuning  $\beta$ , which controls the trade-off between stability and optimal updates. The fidelity after one gradient ascent update step  $\theta' = \theta + \alpha G_\beta(\theta)$  with arbitrary learning rate  $\alpha$  is given by (derivation in Supplemental materials)

$$K_t(\theta') = K_t(\theta) \exp \left[ -\frac{1}{4} (\alpha^2 \nabla K_t^T(\theta) \mathcal{F}^{1-2\beta}(\theta) \nabla K_t(\theta) + 2\alpha \Delta\theta^T \mathcal{F}^{1-\beta}(\theta) \nabla K_t(\theta)) \right]. \quad (6)$$

We find that for  $\beta \leq \frac{1}{2}$ , Eq. (6) is free of any  $\mathcal{F}^{-\delta}$  with negative exponent, which could cause instabilities. We propose that gradient ascent with  $\beta = \frac{1}{2}$  and  $G_{\frac{1}{2}}(\theta) = \mathcal{F}^{-\frac{1}{2}} \nabla K_t(\theta)$  is the optimal choice that combines stability and using quantum geometric information as much as possible.

Next, we show the optimal adaptive learning rates for gradient ascent (derivation in Supplemental materials). The initial update rule is given by  $\theta_1 = \theta + \alpha_1 G_\beta(\theta)$  with the learning rate

$$\alpha_1 = \frac{2\sqrt{-\log(K_t(\theta))}}{\sqrt{G_\beta(\theta)^T \mathcal{F}(\theta) G_\beta(\theta)}}. \quad (7)$$

If the PQC is unable to represent the target state perfectly, i.e.  $\max_\theta |\langle \psi(\theta) | \psi_t \rangle|^2 = K_0 < 1$ , where  $K_0$  is the maximal possible fidelity, we can adjust the step using  $K_t(\theta_1)$ . Then, the updated parameter  $\theta'_t$  is given by  $\theta'_t = \theta + \alpha_t G_\beta(\theta)$  with the adaptive learning rate

$$\alpha_t = \frac{1}{2} \left( \frac{4}{\alpha_1 G_\beta(\theta) \mathcal{F}(\theta) G_\beta(\theta)} \log \left( \frac{K_t(\theta_1)}{K_t(\theta)} \right) + \alpha_1 \right). \quad (8)$$

This concludes one step of gradient ascent. By setting  $\theta = \theta'_t$  and repeating above steps, the next iteration of gradient ascent can be performed.

For a given fidelity  $K_t(\theta)$ , we can derive the variance of the gradient analytically (see Supplemental materials)

$$\text{var}(\partial_k K_t(\theta)) = \langle \langle (\partial_k K_t(\theta))^2 \rangle_{\Delta\theta} \rangle_k - \langle \langle \partial_k K_t(\theta) \rangle_{\theta} \rangle_k^2 = \frac{1}{M} \frac{\text{Tr}(\mathcal{F}(\theta)^2)}{\text{Tr}(\mathcal{F}(\theta))} K_t(\theta)^2 \log \left[ \frac{K_0}{K_t(\theta)} \right], \quad (9)$$

where the average is first taken over distance  $\Delta\theta = \theta - \theta_t$  and then over the gradient indices  $k$ . The variance is maximized for fidelity  $K_t(\theta) \approx 0.6K_0$ . For a fixed fidelity  $K_t(\theta)$ , the variance decreases linearly with number of parameters  $M$  and is independent of qubit number  $N$ . With  $\text{Tr}(\mathcal{F}(\theta)^2) \geq \frac{\text{Tr}(\mathcal{F}(\theta))^2}{M}$ , we give the lower bound of the variance

$$\text{var}(\partial_k K_t(\theta)) \geq \frac{\text{Tr}(\mathcal{F}(\theta))}{M^2} K_t(\theta)^2 \log \left[ \frac{K_0}{K_t(\theta)} \right]. \quad (10)$$

We find a good match between Eq. (9) and simulated results in Fig. 2b for different types of PQCs, which improves with more qubits. It starts deviating from the analytic result when the variance of the gradient becomes

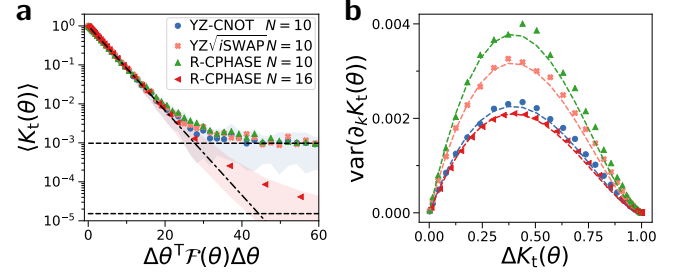


FIG. 2. a) Average fidelity  $\langle K_t(\theta) \rangle$  as function of parameter norm  $\Delta\theta^T \mathcal{F}(\theta) \Delta\theta$ , with distance  $\Delta\theta = \theta - \theta_t$  and target parameters  $\theta_t$ . Shaded area is the 20-th and 80-th percentile of the fidelity. We find a good match with the Gaussian kernel (Eq. (4), dash-dotted line). For large norm, we see the fidelity converges to the fidelity given by random states  $\langle K_{\text{rand}} \rangle = \frac{1}{2^N}$  (dashed lines). We use three different PQCs with randomized parameters, which are defined in the Supplemental materials. Number of layers  $p = 20$  for R-CPHASE  $N = 10$ ,  $p = 16$  for  $N = 16$ , else  $p = 10$ . Average over 50 random instances of  $\theta_t$ . b) Variance of gradient  $\text{var}(\partial_k K_t(\theta))$  against infidelity  $\Delta K_t(\theta)$  for different types of PQCs. Dashed lines are the analytic formula Eq. (9) for the variance.

close to the one given by a state sampled from a deep PQC with  $\text{var}(\nabla K_t(\theta_{\text{rand}})) = \frac{1}{2^{2N+1}}$  [7] (see Supplemental materials).

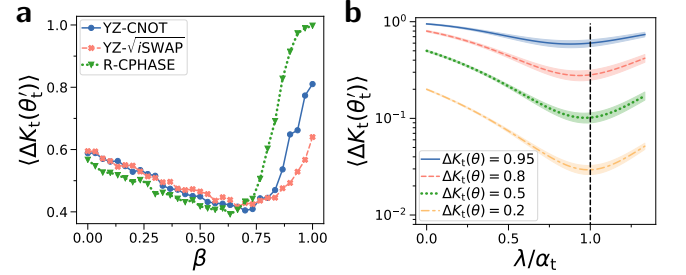


FIG. 3. a) Average infidelity  $\langle \Delta F(\theta'_t) \rangle$  after one step of gradient ascent with adaptive learning rate Eq. (8) plotted against factor  $\beta$  of the GQNG (Eq. (5)) for different types of PQCs. Initial infidelity is  $\Delta K_t(\theta) = 0.9$ . Infidelity is minimal around  $\beta \approx 0.6$ . b)  $\langle \Delta K_t(\theta'_t) \rangle$  (Eq. (1)) plotted against learning rate  $\lambda$ . We use gradient ascent update  $\theta'_t = \theta + \lambda G_{\frac{1}{2}}(\theta)$  with GQNG.  $\lambda$  is plotted normalized in respect to adaptive learning rate  $\alpha_t$  (Eq. (8)), shown as vertical dashed line. Curves show various initial infidelities  $\Delta K_t(\theta)$ , with the shaded area being the standard deviation of  $\Delta K_t(\theta'_t)$ . Infidelity is averaged over 50 random instances of  $\theta_t$  for the YZ-CNOT PQC.

*Results*— We now demonstrate the performance of our VQA using numerical simulations [34, 35] with various types of expressive PQCs [22, 36]. In Fig. 3a, we plot the average infidelity after a single step of gradient ascent  $\langle \Delta K_t(\theta'_t) \rangle$  (Eq. (1)) against  $\beta$  of the GQNG (Eq. (5)). Initially, the infidelity decreases with increasing  $\beta$  as more information from the QFIM is used. However, be-

yond  $\beta > 0.6$  we observe a sharp increase of infidelity for all types of PQCs studied due to an ill-conditioned inverse of the QFIM.

In Fig.3b, we show the average infidelity after a single step of gradient ascent with the GQNG as function of learning rate  $\lambda$  for different initial infidelities  $\Delta K_t(\boldsymbol{\theta})$ . We find that  $\alpha_t$  as calculated by Eq. (8) gives nearly the best learning rate even for larger infidelities. We find the same result when using the regular gradient instead of the GQNG as well as for target states that cannot be perfectly represented by the PQC (see Supplemental materials).

In Fig.4a, we show  $\langle \Delta K_t(\boldsymbol{\theta}'_t) \rangle$  after one step of adaptive gradient ascent against initial infidelity  $\Delta K_t(\boldsymbol{\theta})$  with the standard gradient ( $\beta = 0$ , upper curves) and the GQNG ( $\beta = \frac{1}{2}$ , lower curves). GQNG has lower infidelities compared to the standard gradient and the different PQCs have nearly the same trajectory. We numerically find that the data is fitted well with  $\Delta K_t(\boldsymbol{\theta}'_t) = \frac{c}{4} \Delta \boldsymbol{\theta}^T \mathcal{F} \Delta \boldsymbol{\theta} = -c \log[1 - \Delta K_t(\boldsymbol{\theta})]$ .

In Fig.4b, we plot  $\langle \Delta K_t(\boldsymbol{\theta}'_t) \rangle$  against number of iterations of gradient ascent. We compare our adaptive training method using the GQNG with other established methods. GQNG with adaptive learning rate (A-GQNG with  $\beta = \frac{1}{2}$ ) outperforms other investigated methods and provides more than one order of magnitude smaller infidelities. It consistently performs well for different random instances, demonstrating a very low standard deviation in fidelity. We note that gradient ascent with adaptive learning rate and standard gradient (A-G with  $\beta = 0$ ) still performs well, comparable to Adam and LBFGS. The QNG is unable to converge. Interestingly, standard gradient ascent with fixed learning rates (G) performs initially better than GQNG with fixed learning rates (GQNG), however GQNG performs better at later iterations as the GQNG requires different learning rates depending on the infidelity and QFIM. This highlights the importance of adaptive learning rates in training VQAs. See Supplemental materials for further training data with other PQCs, different initial infidelities and logarithmic plots.

*Discussion*— We showed how to optimally train a PQC to represent a target quantum state. We found that the fidelity of quantum states can form Gaussian kernels and used this relation to derive the optimal adaptive learning rates for gradient ascent. The best direction for the gradient updates is provided by the GQNG (Eq. (5)) with  $\beta = \frac{1}{2}$  and  $G_{\frac{1}{2}}(\boldsymbol{\theta}) = \mathcal{F}^{-\frac{1}{2}} \nabla K_t(\boldsymbol{\theta})$ . It uses the quantum geometric information as much as possible while avoiding the problems due to an ill-conditioned QFIM. We apply these methods to train different expressive PQCs that are able to represent a wide range of quantum states and are commonly used for VQAs [22, 36]. Combining adaptive learning rates and the GQNG, we yield a lower number of iterations and an order of magnitude improvement in accuracy compared to other methods. This approach can

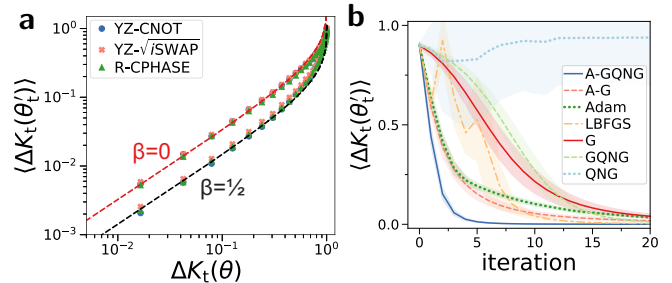


FIG. 4. **a)** Mean infidelity  $\langle \Delta K_t(\boldsymbol{\theta}'_t) \rangle$  after one step of adaptive gradient ascent against initial infidelity  $\Delta K_t(\boldsymbol{\theta})$ . We show for regular gradient ( $\beta = 0$ , upper curves) and GQNG ( $\beta = \frac{1}{2}$ , lower curves) for various types of PQCs. The red and black curves are fits with  $\Delta K_t(\boldsymbol{\theta}'_t) = \frac{c}{4} \Delta \boldsymbol{\theta}^T \mathcal{F} \Delta \boldsymbol{\theta} = -c \log[1 - \Delta K_t(\boldsymbol{\theta})]$ , with  $c(\beta = \frac{1}{2}) = 0.14$  and  $c(\beta = 0) = 0.32$ . **b)** Mean infidelity  $\langle \Delta K_t(\boldsymbol{\theta}'_t) \rangle$  against number of iterations of gradient ascent. Shaded area is the standard deviation over 50 instances of training. We compare different optimization methods against each other. We find that our adaptive gradient ascent with GQNG (A-QNG) performs best by a large margin, followed by adaptive method with regular gradient (A-G). Standard optimization methods such as Adam ( $\gamma = 0.1$ ) and LBFGS perform a bit worse than A-G. Standard gradient ascent with regular gradient (G,  $\alpha = 0.5$ ) performs initially better than the standard GQNG (GQNG,  $\alpha = 0.5$ ), but QNG is superior for more iterations. QNG is unable to converge. Initial infidelity is  $\Delta K_t(\boldsymbol{\theta}) = 0.9$ , training is averaged over 50 random instances of  $\boldsymbol{\theta}_t$ , PQC is YZ-CNOT,  $N = 10$  and  $p = 10$ .

be directly applied to a large range of VQAs, which have a subroutine that requires learning quantum states using the fidelity [23–28, 37]. Future work can extend our methods to other cost functions such as Hamiltonians or the Hilbert-Schmidt test [38]. The QFIM  $\mathcal{F}$  needed for our method can be efficiently approximated using quantum computers [21, 32, 39, 40] as well as efficiently calculated classically [41].

While we discussed training in the context of PQC and VQAs, we note that our method is general and can also be applied for the control of quantum systems [42]. Here, the task is to find the optimal driving protocol to generate a particular quantum state. By partitioning the driving protocol into discrete timesteps, the unitary that parameterizes the driving protocol has the form of a PQC, with the parameters being the amplitude of the driving protocol. Numerical optimization methods such as GRAPE [43] use gradients to find the best possible driving protocol. By using our adaptive learning rates and GQNG one could enhance those methods to find better protocols in a faster way.

A common feature of the cost function in many PQCs is that they form a narrow gorge, i.e. the cost function deviates from its mean only in an exponentially small parameter space [8, 44]. These narrow gorges directly imply the existence of barren plateaus, i.e. the vari-

ance of the gradient vanishes exponentially with number of qubits, making training difficult for large quantum computers [7, 44]. Optimizing the PQC to represent a random state  $|\psi_{\text{rand}}\rangle \in \mathcal{SU}(2^N)$  suffers from barren plateaus, which appear independent of the depth of the PQC [8]. The Gaussian kernel gives us now a functional description of the narrow gorge for the fidelity as cost function and allows us to calculate the variance of the gradients. We can ensure trainability and avoid the barren plateau problem by demanding that the state to be learned  $|\psi_t\rangle$  is not random, but has a lower bounded fidelity with the initial state  $K_t(\theta) > \gamma$ , where  $\gamma$  is the lower bound. We further assume that we are not too close to the optimal solution with  $K_t(\theta) < 0.6K_0$  where  $K_0$  is the maximal possible fidelity. Then, Eq. (10) tells us that the variance of the gradient is lower bounded by  $\text{var}(\nabla K_t(\theta)) \geq \frac{\text{Tr}(\mathcal{F})}{M^2} \log(\frac{K_0}{\gamma})\gamma^2$ . In particular, the lower bound of the variance is independent of the number of qubits  $N$  of the quantum computer and therefore the gradient does not vanish even when we scale up  $N$ . We now derive  $\gamma$  for the projected variational quantum dynamics method [23, 24]. This algorithm simulates the evolution of the state  $|\psi(\theta)\rangle$  with a Hamiltonian  $H$  (see Supplemental materials for training examples). It evolves the PQC using a single Trotter step with time  $\Delta t$  and then variationally learns to represent the evolved state  $|\psi_t\rangle = \exp(-iH\Delta t)|\psi(\theta)\rangle$  via the fidelity as cost function. This process is then repeated  $N_T$  times to evolve for a total time  $T = N_T\Delta t$ . Here, we find  $\gamma = 1 - \frac{1}{4}(\Delta E\Delta t)^2$  with  $\Delta E$  being the energy difference between the largest and smallest eigenenergies of  $H$  whose eigenstates have non-zero overlap with  $|\psi(\theta)\rangle$  (see Supplemental materials). By choosing a small enough  $\Delta t$  and  $\Delta E$ , one can ensure sufficiently large gradients and that the VQA is free of barren plateaus. This opens up the possibility to train these VQAs on large-scale quantum computers. An interesting application would be to simulate the dynamics of complicated many-body systems that are beyond the reach of current classical simulation methods. To reach this goal, future work has to engineer PQCs that are able to represent the time evolved states even for large number of qubits. Adaptively chosen PQCs [45] or PQCs tailored to the specific problem could enhance the representation power. Hybrid states as linear combination of quantum states generated using the problem Hamiltonian could systematically create an ansatz suited for the problem [13–15]. We note that training VQAs without a lower bounded fidelity is expected to be difficult, as most likely training will be stuck in the barren plateau. In this case, other types of cost function may provide a way out of the barren plateau [8].

As a tangential observation, we note that Eq. (9) enables us to calculate  $\text{Tr}(\mathcal{F}^2)$  by measuring the variance of the gradients.

Finally, our results have direct implications for quantum machine learning, which utilizes quantum features

to enhance machine learning. Here, data is embedded as parameters of the PQC and the fidelity of the quantum states is used as a nonlinear feature map [46–48]. The Gaussian (or radial basis function) kernel we provide is such a nonlinear feature map, which has important applications in various classical machine learning models such as support vector machines [49]. In a quantum setting, these kernels have been so far only proposed with coherent states [50–52]. As advantage compared to coherent states, PQCs can adjust the QFIM and the weight matrix of the Gaussian kernel by changing the structure of the PQC [22]. Given that these kernels can be efficiently computed classically, they are unlikely to provide a direct quantum advantage from data in machine learning [47, 51, 53]. However, with increasing distance in parameter space the approximation as Gaussian is less accurate and the kernel may acquire the features needed to provide quantum advantage [53]. The kernel could be immediately realized with current quantum hardware for tasks in quantum machine learning [47, 48, 54, 55] and Gaussian processes [52, 56] to provide novel applications of quantum computers.

Python code for the numerical calculations are available [57].

*Acknowledgements*— We acknowledge discussions with Kiran Khosla, Christopher Self and Alistair Smith. This work is supported by a Samsung GRC project and the UK Hub in Quantum Computing and Simulation, part of the UK National Quantum Technologies Programme with funding from UKRI EPSRC grant EP/T001062/1.

---

\* [thaug@ic.ac.uk](mailto:thaug@ic.ac.uk)

- [1] J. Preskill, Quantum computing in the nisq era and beyond, *Quantum* **2**, 79 (2018).
- [2] K. Bharti, A. Cervera-Lierta, T. H. Kyaw, T. Haug, S. Alperin-Lea, A. Anand, M. Degroote, H. Heimonen, J. S. Kottmann, T. Menke, W.-K. Mok, S. Sim, L.-C. Kwek, and A. Aspuru-Guzik, Noisy intermediate-scale quantum (nisq) algorithms, *arXiv:2101.08448* (2021).
- [3] A. Peruzzo, J. McClean, P. Shadbolt, M.-H. Yung, X.-Q. Zhou, P. J. Love, A. Aspuru-Guzik, and J. L. Obrien, A variational eigenvalue solver on a photonic quantum processor, *Nature communications* **5**, 4213 (2014).
- [4] A. Kandala, A. Mezzacapo, K. Temme, M. Takita, M. Brink, J. M. Chow, and J. M. Gambetta, Hardware-efficient variational quantum eigensolver for small molecules and quantum magnets, *Nature* **549**, 242 (2017).
- [5] J. R. McClean, J. Romero, R. Babbush, and A. Aspuru-Guzik, The theory of variational hybrid quantum-classical algorithms, *New Journal of Physics* **18**, 023023 (2016).
- [6] M. Cerezo, A. Arrasmith, R. Babbush, S. C. Benjamin, S. Endo, K. Fujii, J. R. McClean, K. Mitarai, X. Yuan, L. Cincio, *et al.*, Variational quantum algorithms, *arXiv preprint arXiv:2012.09265* (2020).

[7] J. R. McClean, S. Boixo, V. N. Smelyanskiy, R. Babbush, and H. Neven, Barren plateaus in quantum neural network training landscapes, *Nature communications* **9**, 4812 (2018).

[8] M. Cerezo, A. Sone, T. Volkoff, L. Cincio, and P. J. Coles, Cost function dependent barren plateaus in shallow parametrized quantum circuits, *Nature Communications* **12**, 1 (2021).

[9] C. O. Marrero, M. Kieferová, and N. Wiebe, Entanglement induced barren plateaus, arXiv:2010.15968 (2020).

[10] S. Wang, E. Fontana, M. Cerezo, K. Sharma, A. Sone, L. Cincio, and P. J. Coles, Noise-induced barren plateaus in variational quantum algorithms, arXiv:2007.14384 (2020).

[11] L. Bittel and M. Kliesch, Training variational quantum algorithms is np-hard – even for logarithmically many qubits and free fermionic systems, arXiv:2101.07267 (2021).

[12] K. Bharti, Quantum assisted eigensolver, arXiv:2009.11001 (2020).

[13] K. Bharti and T. Haug, Quantum assisted simulator, arXiv:2011.06911 (2020).

[14] K. Bharti and T. Haug, Iterative quantum assisted eigensolver, arXiv:2010.05638 (2020).

[15] T. Haug and K. Bharti, Generalized quantum assisted simulator, arXiv:2011.14737 (2020).

[16] J. W. Z. Lau, T. Haug, L. C. Kwek, and K. Bharti, Nisq algorithm for hamiltonian simulation via truncated taylor series, arXiv:2103.05500 (2021).

[17] K. H. Lim, T. Haug, L. C. Kwek, and K. Bharti, Fast-forwarding with nisq processors without feedback loop, arXiv:2104.01931 (2021).

[18] J. Stokes, J. Izaac, N. Killoran, and G. Carleo, Quantum natural gradient, *Quantum* **4**, 269 (2020).

[19] B. Koczor and S. C. Benjamin, Quantum natural gradient generalised to non-unitary circuits, arXiv preprint arXiv:1912.08660 (2019).

[20] N. Yamamoto, On the natural gradient for variational quantum eigensolver, arXiv:1909.05074 (2019).

[21] J. Gacon, C. Zoufal, G. Carleo, and S. Woerner, Simultaneous perturbation stochastic approximation of the quantum fisher information, arXiv:2103.09232 (2021).

[22] T. Haug, K. Bharti, and M. Kim, Capacity and quantum geometry of parametrized quantum circuits, arXiv:2102.01659 (2021).

[23] M. Otten, C. L. Cortes, and S. K. Gray, Noise-resilient quantum dynamics using symmetry-preserving ansatzes, arXiv preprint arXiv:1910.06284 (2019).

[24] S. Barison, F. Vicentini, and G. Carleo, An efficient quantum algorithm for the time evolution of parameterized circuits, arXiv:2101.04579 (2021).

[25] J. Gibbs, K. Gili, Z. Holmes, B. Commeau, A. Arrasmith, L. Cincio, P. J. Coles, and A. Sornborger, Long-time simulations with high fidelity on quantum hardware, arXiv:2102.04313 (2021).

[26] Z. Holmes, A. Arrasmith, B. Yan, P. J. Coles, A. Albrecht, and A. T. Sornborger, Barren plateaus preclude learning scramblers, arXiv:2009.14808 (2020).

[27] M. Benedetti, D. Garcia-Pintos, O. Perdomo, V. Leyton-Ortega, Y. Nam, and A. Perdomo-Ortiz, A generative modeling approach for benchmarking and training shallow quantum circuits, *npj Quantum Information* **5**, 1 (2019).

[28] J. Romero, J. P. Olson, and A. Aspuru-Guzik, Quantum autoencoders for efficient compression of quantum data, *Quantum Sci. Technol.* **2**, 045001 (2017).

[29] O. Higgott, D. Wang, and S. Brierley, Variational quantum computation of excited states, *Quantum* **3**, 156 (2019).

[30] J. Liu, H. Yuan, X.-M. Lu, and X. Wang, Quantum fisher information matrix and multiparameter estimation, *Journal of Physics A: Mathematical and Theoretical* **53**, 023001 (2019).

[31] J. J. Meyer, Fisher information in noisy intermediate-scale quantum applications, 2103.15191 (2021).

[32] B. van Straaten and B. Koczor, Measurement cost of metric-aware variational quantum algorithms, arXiv:2005.05172 (2020).

[33] W. G. Brown and L. Viola, Convergence rates for arbitrary statistical moments of random quantum circuits, *Physical review letters* **104**, 250501 (2010).

[34] X.-Z. Luo, J.-G. Liu, P. Zhang, and L. Wang, Yao. jl: Extensible, efficient framework for quantum algorithm design, *Quantum* **4**, 341 (2020).

[35] J. R. Johansson, P. D. Nation, and F. Nori, Qutip: An open-source python framework for the dynamics of open quantum systems, *Computer Physics Communications* **183**, 1760 (2012).

[36] S. Sim, P. D. Johnson, and A. Aspuru-Guzik, Expressibility and entangling capability of parameterized quantum circuits for hybrid quantum-classical algorithms, *Advanced Quantum Technologies* **2**, 1900070 (2019).

[37] T. Jones, S. Endo, S. McArdle, X. Yuan, and S. C. Benjamin, Variational quantum algorithms for discovering hamiltonian spectra, *Physical Review A* **99**, 062304 (2019).

[38] S. Khatri, R. LaRose, A. Poremba, L. Cincio, A. T. Sornborger, and P. J. Coles, Quantum-assisted quantum compiling, *Quantum* **3**, 140 (2019).

[39] M. Cerezo, A. Sone, J. L. Beckey, and P. J. Coles, Sub-quantum fisher information, arXiv preprint arXiv:2101.10144 (2021).

[40] J. L. Beckey, M. Cerezo, A. Sone, and P. J. Coles, Variational quantum algorithm for estimating the quantum fisher information, arXiv:2010.10488 (2020).

[41] T. Jones, Efficient classical calculation of the quantum natural gradient, arXiv preprint arXiv:2011.02991 (2020).

[42] S. J. Glaser, U. Boscain, T. Calarco, C. P. Koch, W. Köckenberger, R. Kosloff, I. Kuprov, B. Luy, S. Schirmer, T. Schulte-Herbrüggen, *et al.*, Training schrödinger’s cat: quantum optimal control, *The European Physical Journal D* **69**, 1 (2015).

[43] S. Machnes, U. Sander, S. J. Glaser, P. De Fouquière, A. Gruslys, S. Schirmer, and T. Schulte-Herbrüggen, Comparing, optimizing, and benchmarking quantum-control algorithms in a unifying programming framework, *Physical Review A* **84**, 022305 (2011).

[44] A. Arrasmith, Z. Holmes, M. Cerezo, and P. J. Coles, Equivalence of quantum barren plateaus to cost concentration and narrow gorges, arXiv:2104.05868 (2021).

[45] H. R. Grimsley, S. E. Economou, E. Barnes, and N. J. Mayhall, An adaptive variational algorithm for exact molecular simulations on a quantum computer, *Nature communications* **10**, 1 (2019).

[46] J. Biamonte, P. Wittek, N. Pancotti, P. Rebentrost, N. Wiebe, and S. Lloyd, Quantum machine learning, *Nature* **549**, 195 (2017).

- [47] M. Schuld and N. Killoran, Quantum machine learning in feature hilbert spaces, *Physical review letters* **122**, 040504 (2019).
- [48] M. Schuld, R. Swoke, and J. J. Meyer, Effect of data encoding on the expressive power of variational quantum-machine-learning models, *Physical Review A* **103**, 032430 (2021).
- [49] I. Goodfellow, Y. Bengio, A. Courville, and Y. Bengio, *Deep learning*, Vol. 1 (MIT press Cambridge, 2016).
- [50] R. Chatterjee and T. Yu, Generalized coherent states, reproducing kernels, and quantum support vector machines, *arXiv:1612.03713* (2016).
- [51] M. Schuld, Quantum machine learning models are kernel methods, *arXiv:2101.11020* (2021).
- [52] M. Otten, I. R. Goumire, B. W. Priest, G. F. Chapline, and M. D. Schneider, Quantum machine learning using gaussian processes with performant quantum kernels, *arXiv preprint arXiv:2004.11280* (2020).
- [53] H.-Y. Huang, M. Broughton, M. Mohseni, R. Babbush, S. Boixo, H. Neven, and J. R. McClean, Power of data in quantum machine learning, *arXiv:2011.01938* (2020).
- [54] V. Havlíček, A. D. Córcoles, K. Temme, A. W. Harrow, A. Kandala, J. M. Chow, and J. M. Gambetta, Supervised learning with quantum-enhanced feature spaces, *Nature* **567**, 209 (2019).
- [55] C. Blank, D. K. Park, J.-K. K. Rhee, and F. Petruccione, Quantum classifier with tailored quantum kernel, *npj Quantum Information* **6**, 1 (2020).
- [56] C. E. Rasmussen and C. K. I. Williams, *Gaussian Processes for Machine Learning (Adaptive Computation and Machine Learning)* (The MIT Press, 2005).
- [57] T. Haug, Optimal quantum learning, <https://github.com/txhaug/optimal-quantum-learning>.

### Parameterized quantum circuits

The PQCs used in the main text are described in Fig.5. The PQCs are given by  $\psi(\boldsymbol{\theta}) = U(\boldsymbol{\theta})|0\rangle^{\otimes N} = \prod_{l=p}^1 [W_l V_l(\theta_l)] |0\rangle^{\otimes N}$ , which consist of  $p$  layers of entangling gates  $W_l$  and parameterized rotations  $V_l(\theta_l)$ . The parameters  $\boldsymbol{\theta}$  are chosen randomly.

### Further data

In this section we show further numerical simulations. We compare the adaptive gradient ascent using the GQNG and regular gradient in Fig.6. We find for both types of gradients, the adaptive gradient ascent finds the nearly optimal learning rate.

Now, we choose a target state that cannot be perfectly represented by the PQC, i.e.  $K_0 = \max_{\boldsymbol{\theta}} K_t(\boldsymbol{\theta}) < 1$ . In Fig.7, we investigate the learning rate  $\lambda$  normalized to the optimal one  $\alpha_t$  for  $K_0 = 0.5$ . We find for both types of gradients, the adaptive gradient ascent finds the nearly optimal learning rate.

In Fig.8a, we show the variance of the gradient as function of parameter norm  $\boldsymbol{\theta}^T \mathcal{F} \boldsymbol{\theta}$ . We see a good match with the analytic formula. For large  $\boldsymbol{\theta}^T \mathcal{F} \boldsymbol{\theta}$ , we

see deviation from the analytic result, as the variance of the gradient approaches the value given by a random state sampled from a sufficiently deep PQC with  $\text{var}(\nabla K_t(\boldsymbol{\theta}_{\text{rand}})) = \frac{1}{2^{2N+1}}$  [7].

### Further training data

In this section we show further data for the training of the VQA. We show training of our VQA in Fig.9 for both linear and logarithmic plots for the YZ-CNOT PQC. We see that GQNG with adaptive learning rates provides about one order of magnitude smaller infidelities compared to other methods.

We show further training of our VQA in Fig.10 for for the R-CPHASE PQC. We find similar trajectories as before, however in general the infidelities are a bit higher. This may be related to the fact that the R-CPHASE PQC has a QFIM with more smaller eigenvalues compared to the YZ-CNOT PQC. This may affect training adversely here.

In Fig.11 we show the trajectories for the YZ- $\sqrt{i}$ SWAP PQC.

In Fig.12, we compare GQNG with adaptive learning rate (A-GQNG) against Adam and LBFGS for different values of initial infidelity. We find superior performance for higher infidelities as well.

In Fig.13, we compare training with A-GQNG for different initial infidelities  $\Delta K_t(\boldsymbol{\theta})$ . We can train the PQC even for very high infidelities. Note that the Gaussian kernel approximation breaks down for  $\Delta K_t(\boldsymbol{\theta}) > 1 - \frac{1}{2^N} \approx 0.999$ . However, training is still possible then, although at a slower rate.

Now, again the target state to be learned cannot be perfectly represented by PQC, i.e.  $K_0 = \max_{\boldsymbol{\theta}} K_t(\boldsymbol{\theta}) = 0.5$ . We show the trajectories for the YZ-CNOT PQC in Fig.14. We note that A-GQNG also performs much better than other algorithms in this situation.

### PQC with Gaussian kernel

We show a PQC with Gaussian kernel that can be analytically calculated with the following  $N$  qubit quantum state

$$|\psi(\boldsymbol{\theta})\rangle = \bigotimes_{n=1}^N \left( \cos\left(\frac{\theta_n}{2}\right) |0\rangle + \sin\left(\frac{\theta_n}{2}\right) |1\rangle \right). \quad (11)$$

The fidelity of two states parameterized by  $\boldsymbol{\theta}, \boldsymbol{\theta}'$  is given by

$$K(\boldsymbol{\theta}, \boldsymbol{\theta}') = |\langle \psi(\boldsymbol{\theta}) | \psi(\boldsymbol{\theta}') \rangle|^2 = \prod_{n=1}^N \left( 1 + \frac{1}{2} \cos(\Delta\theta_n) \right) \quad (12)$$

where we define  $\Delta\boldsymbol{\theta} = \boldsymbol{\theta} - \boldsymbol{\theta}'$  as the difference between the two parameter sets. We now assume  $|\Delta\theta_n| \ll 1$  and

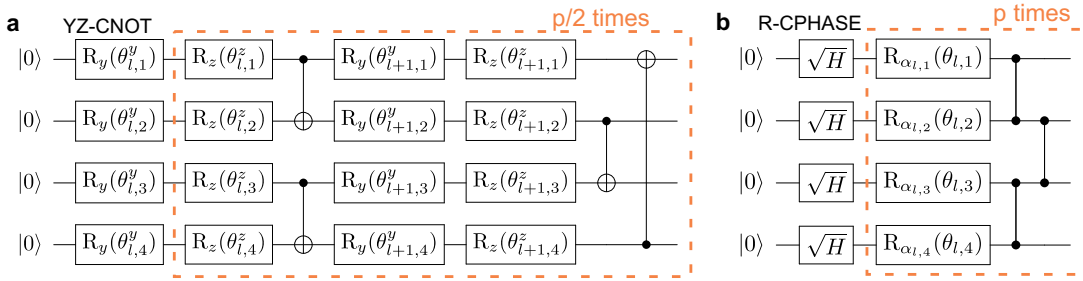


FIG. 5. Description of PQCs used in the main text. **a)** YZ-CNOT consists of  $p$  layers, with each layer having Y and Z rotations applied on each qubit, and CNOT gates between neighboring qubits applied in an alternating fashion. For odd layer number  $l$ , CNOT gate is applied between qubit  $2n - 1$  and  $2n$ , for even  $l$  CNOT is applied on  $2n$  and  $2n + 1$ . For YZ- $\sqrt{i}$ SWAP, the CNOT gates are replaced with  $\sqrt{i}$ SWAP gates. **b)** R-CPHASE PQC, which consists of an initial layer of  $\pi/2$  rotation around the  $y$ -axis, followed by  $p$  layers. Each layer consists of randomly chosen rotations with  $\sigma^x$ ,  $\sigma^y$  or  $\sigma^z$ , followed by CPHASE gates applied as a chain of nearest-neighbors.

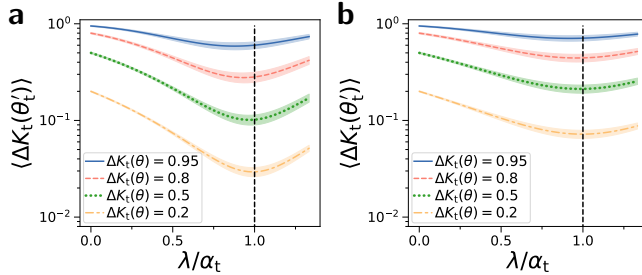


FIG. 6. Average infidelity after one step of gradient ascent step  $\langle \Delta K_t(\theta'_t) \rangle$  (Eq. (1)) plotted against learning rate  $\lambda$ , for gradient ascent update  $\theta'_t = \theta + \lambda G_\beta(\theta)$ .  $\lambda$  is normalized in respect to analytically calculated learning rate  $\alpha_t$  (Eq. (33)), shown as vertical dashed line. Curves show various initial infidelities  $\Delta K_t(\theta)$ , with shaded area being the standard deviation of  $\Delta K_t(\theta'_t)$ . Infidelity averaged over 50 random instances of YZ-CNOT PQC. We show **a)** the GQNG  $\beta = \frac{1}{2}$  and **b)** the regular gradient  $\beta = 0$ .

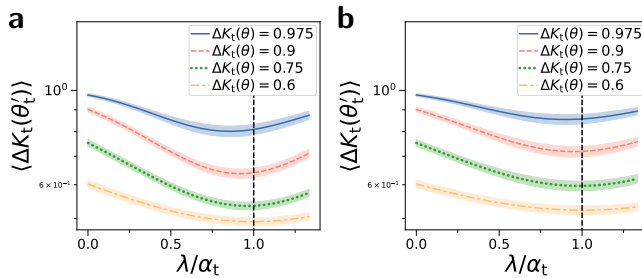


FIG. 7. Target state to be learned cannot be perfectly represented by PQC, i.e.  $K_0 = \max_{\theta} K_t(\theta) = 0.5$ . Average infidelity after one step of gradient ascent step  $\langle \Delta K_t(\theta'_t) \rangle$  (Eq. (1)) plotted against learning rate  $\lambda$ , for gradient ascent update  $\theta'_t = \theta + \lambda G_\beta(\theta)$ .  $\lambda$  is normalized in respect to analytically calculated learning rate  $\alpha_t$ , shown as vertical dashed line. Curves show various initial infidelities  $\Delta K_t(\theta)$ , with shaded area being the standard deviation of  $\Delta K_t(\theta'_t)$ . Infidelity averaged over 50 random instances of YZ-CNOT PQC. We show **a)** the GQNG  $\beta = \frac{1}{2}$  and **b)** the regular gradient  $\beta = 0$ .

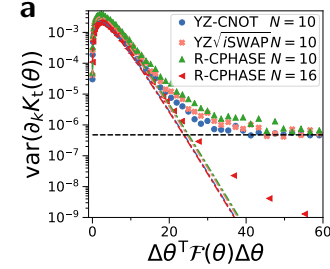


FIG. 8. **a)** Variance of gradient  $\text{var}(\partial_k K_t(\theta))$  against parameter norm  $\Delta \theta^T \mathcal{F}(\theta) \Delta \theta$  for different types of PQCs. Dashed line is the analytic formula Eq. (39) for the variance. The dashed horizontal line is the variance of the gradient for states of a random PQC  $\text{var}(\nabla K_t(\theta_{\text{rand}})) = \frac{1}{2^{N+1}}$  [7]. Number of layers  $p = 20$  for R-CPHASE  $N = 10$ ,  $p = 16$  for  $N = 16$ , else  $p = 10$ . Average over 50 random instances of  $\theta_t$ .

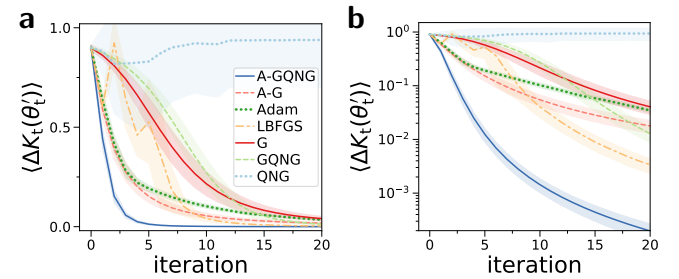


FIG. 9. Training with YZ-CNOT PQC. **a)** Linear Plot **b)** Logarithmic plot. Mean infidelity  $\langle \Delta K_t(\theta'_t) \rangle$  against number of iterations of gradient ascent. Shaded area is the standard deviation over 50 instances of training. We compare different optimization methods against each other. We find that our adaptive gradient ascent with GQNG (A-QNG) performs best by a large margin, followed by adaptive method with regular gradient (A-G). Standard optimization methods such as Adam and LBFGS perform a bit worse than A-G. Standard gradient ascent with regular gradient (G) performs initially better than the GQNG, but GQNG is superior for more iterations. QNG is unable to converge due to stability issues. Initial infidelity is  $\Delta K_t(\theta) = 0.9$ ,  $N = 10$  and  $p = 10$ .

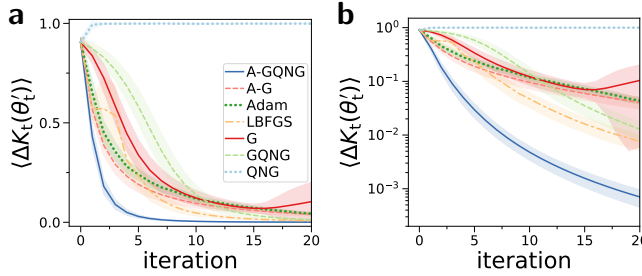


FIG. 10. Training with R-CPHASE PQC. **a)** Linear Plot **b)** Logarithmic plot. Mean infidelity  $\langle \Delta K_t(\theta'_t) \rangle$  against number of iterations of gradient ascent. Initial infidelity is  $\Delta K_t(\theta) = 0.9$ ,  $N = 10$  and  $p = 20$ .

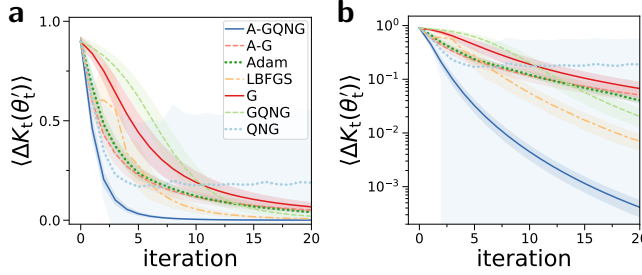


FIG. 11. Training with YZ- $\sqrt{i}$ SWAP PQC. **a)** Linear Plot **b)** Logarithmic plot. Mean infidelity  $\langle \Delta K_t(\theta'_t) \rangle$  against number of iterations of gradient ascent. Initial infidelity is  $\Delta K_t(\theta) = 0.9$ ,  $N = 10$  and  $p = 10$ .

that all the differences of the parameters are equal  $\Delta\theta_1 = \dots = \Delta\theta_N$ . We then find in the limit of many qubits  $N$

$$K(\theta, \theta') \approx \prod_{n=1}^N \left(1 - \frac{1}{4} \Delta\theta_n^2\right) \xrightarrow{N \rightarrow \infty} \exp\left(-\frac{1}{4} \Delta\theta^T \Delta\theta\right). \quad (13)$$

The QFIM of above model is  $\mathcal{F}(\theta) = I$ ,  $I$  being the identity matrix. We can now modify the model to describe a generic PQC with the QFIM  $\mathcal{F}$ . We now assume that

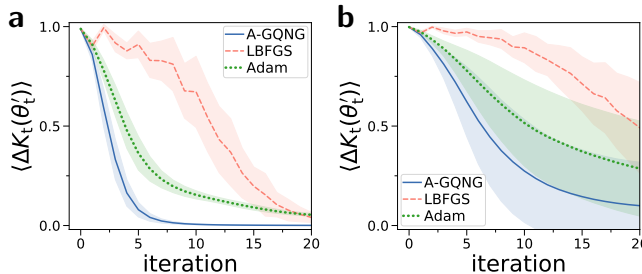


FIG. 12. Mean infidelity  $\langle \Delta K_t(\theta'_t) \rangle$  against number of iterations of gradient ascent. Shaded area is the standard deviation over 50 instances of training. We show compare GQNG with adaptive learning rate against Adam and L-BFGS. **a)** Initial infidelity  $\Delta K_t(\theta) = 0.99$  **b)**  $\Delta K_t(\theta) = 0.999$ . The PQC used is YZ-CNOT with  $N = 10$  and  $p = 10$ .

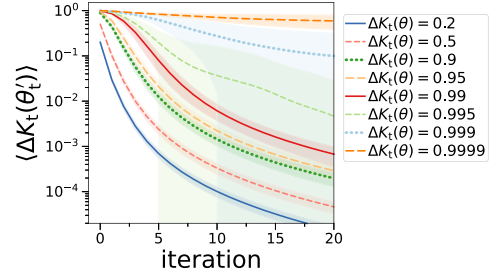


FIG. 13. Different initial infidelities  $\Delta K_t(\theta)$  for A-GQNG. Mean infidelity  $\langle \Delta K_t(\theta'_t) \rangle$  against number of iterations of gradient ascent. Shaded area is the standard deviation over 50 instances of training. The PQC is YZ-CNOT with  $N = 10$  and  $p = 10$ .

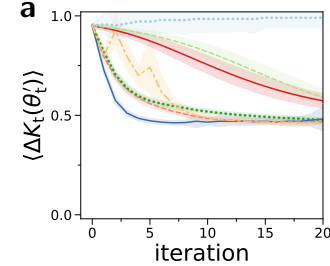


FIG. 14. Training with YZ-CNOT PQC where target state cannot be learned perfectly, i.e.  $K_0 = \max_\theta K_t(\theta) = 0.5$ . Mean infidelity  $\langle \Delta K_t(\theta'_t) \rangle$  against number of iterations of gradient ascent for different optimization routines (see other Figures for legend). Initial infidelity is  $\Delta K_t(\theta) = 0.9$ ,  $N = 10$  and  $p = 10$ .

the parameters of the PQC  $\theta$  are not independent, but are related via  $\theta = \mathcal{F}^{\frac{1}{2}}\mu$ , where  $\mu$  is some  $N$  dimensional parameter. We find for the transformed parameters  $\mu$

$$K(\mu, \mu') \approx \exp\left(-\frac{1}{4} \Delta\mu^T \mathcal{F} \Delta\mu\right), \quad (14)$$

where  $\Delta\mu = \mu - \mu'$  and we used  $|\mathcal{F}^{\frac{1}{2}}\mu|^2 = \mu^T \mathcal{F} \mu$ . A first order Taylor expansion gives us

$$K(\mu, \mu') \approx \exp\left(-\frac{1}{4} \Delta\mu^T \mathcal{F} \Delta\mu\right) \approx 1 - \frac{1}{4} \Delta\mu^T \mathcal{F} \Delta\mu, \quad (15)$$

which is the relation between fidelity and parameter distance for the QFIM [30, 31].

### Generalized quantum natural gradient

For gradient ascent, we propose the generalized quantum natural gradient (GQNG)

$$G_\beta(\theta) = \mathcal{F}^{-\beta}(\theta) \nabla K_t(\theta), \quad (16)$$

with  $\beta \in [0, 1]$ , the derivative of the fidelity  $\nabla K_t(\theta)$  and the QFIM  $\mathcal{F}(\theta)$ . Standard gradient ascent is

$G_0(\boldsymbol{\theta}) = \nabla K_t(\boldsymbol{\theta})$ , whereas the QNG is  $G_1(\boldsymbol{\theta}) = \mathcal{F}^{-1}(\boldsymbol{\theta})\nabla K_t(\boldsymbol{\theta})$  [18, 20]. The standard gradient is reliable, however it can require many update steps before convergence. While the QNG in theory moves the state optimally in parameter space, we find that in practice it is highly unstable and often unable to converge. We trace this instability back to the inverse of the QFIM  $\mathcal{F}^{-1}(\boldsymbol{\theta})$ , which when ill conditioned is highly sensitive to small changes in parameter  $\boldsymbol{\theta}$ .  $\beta$  allows us to tune the trade-off between stability and optimal updates. With the Gaussian kernel, a gradient ascent update  $\boldsymbol{\theta}' = \boldsymbol{\theta} + \alpha G_\beta(\boldsymbol{\theta})$  gives us the fidelity

$$K_t(\boldsymbol{\theta}') = K_0 \exp\left[-\frac{1}{4}(\Delta\boldsymbol{\theta} + \alpha G_\beta(\boldsymbol{\theta}))^\top \mathcal{F}(\boldsymbol{\theta})(\Delta\boldsymbol{\theta} + \alpha G_\beta(\boldsymbol{\theta}))\right], \quad (17)$$

where  $K_0$  is the maximal possible fidelity and  $\Delta\boldsymbol{\theta} = \boldsymbol{\theta} - \boldsymbol{\theta}_t$ . For convenience, in the following we do not explicitly write the  $\boldsymbol{\theta}$  parameter for  $\mathcal{F}(\boldsymbol{\theta})$  and  $\nabla K_t(\boldsymbol{\theta})$

$$\begin{aligned} K_t(\boldsymbol{\theta}') &= K_t(\boldsymbol{\theta}) \exp\left[-\frac{\alpha}{4}(\alpha G_\beta^\top \mathcal{F} G_\beta + G_\beta^\top \mathcal{F} \Delta\boldsymbol{\theta} + \Delta\boldsymbol{\theta}^\top \mathcal{F} G_\beta)\right] \\ &= K_t(\boldsymbol{\theta}) \exp\left[-\frac{\alpha}{4}(\alpha \nabla K_t^\top \mathcal{F}^{1-2\beta} \nabla K_t + 2\Delta\boldsymbol{\theta}^\top \mathcal{F}^{1-\beta} \nabla K_t)\right], \end{aligned}$$

where we used  $\mathcal{F}^\top = \mathcal{F}$ . For choice  $\beta \leq \frac{1}{2}$ , the updated fidelity avoids any  $\mathcal{F}^{-\delta}$  with negative exponent, which could cause instabilities. Thus, we propose that gradient ascent with  $\beta = \frac{1}{2}$  and  $G_{\frac{1}{2}}(\boldsymbol{\theta}) = \mathcal{F}^{-\frac{1}{2}} \nabla K_t(\boldsymbol{\theta})$  is the optimal choice, as it combines stability with using quantum geometric information as much as possible.

### Gradient update rule

We would like to find  $\boldsymbol{\theta}_t = \operatorname{argmax}_{\boldsymbol{\theta}} |\langle \psi(\boldsymbol{\theta}) | \psi_t \rangle|^2$ . First, we assume that  $\max_{\boldsymbol{\theta}} |\langle \psi(\boldsymbol{\theta}) | \psi_t \rangle|^2 = K_0 = 1$ , i.e. the PQC is able to perfectly represent the state. We relax  $K_0 < 1$  further below. For the initial parameter  $\boldsymbol{\theta}$  we have a fidelity  $K_t(\boldsymbol{\theta})$ . Gradient ascent with the GQNG utilizes the update rule for the next parameter  $\boldsymbol{\theta}_1$

$$\boldsymbol{\theta}_1 = \boldsymbol{\theta} + \alpha_1 G_\beta(\boldsymbol{\theta}), \quad (18)$$

with learning rate  $\alpha_1$  and GQNG  $G_\beta(\boldsymbol{\theta}) = \mathcal{F}^{-\beta}(\boldsymbol{\theta})\nabla K_t(\boldsymbol{\theta})$ . We assume now that the fidelity follows a Gaussian kernel, and we would like to choose  $\alpha_1$  such that this update is as close as possible to the correct solution  $\boldsymbol{\theta}_1 \approx \boldsymbol{\theta}_t$ . Given the Gaussian kernel, we have

$$K_t(\boldsymbol{\theta}) = e^{-\frac{1}{4}\Delta\boldsymbol{\theta}^\top \mathcal{F}(\boldsymbol{\theta})\Delta\boldsymbol{\theta}}. \quad (19)$$

where we defined the distance between target parameter and initial parameter  $\Delta\boldsymbol{\theta} = \boldsymbol{\theta}_t - \boldsymbol{\theta}$ . We then find by applying the logarithm

$$-4 \log(K_t(\boldsymbol{\theta})) = \Delta\boldsymbol{\theta}^\top \mathcal{F}(\boldsymbol{\theta})\Delta\boldsymbol{\theta}. \quad (20)$$

A reordering of Eq. (18) gives us

$$\Delta\boldsymbol{\theta} = \alpha_1 G_\beta(\boldsymbol{\theta}) \quad (21)$$

We now multiply both sides with  $\mathcal{F}^{\frac{1}{2}}(\boldsymbol{\theta})$  and get

$$\mathcal{F}^{\frac{1}{2}}(\boldsymbol{\theta})\Delta\boldsymbol{\theta} = \alpha_1 \mathcal{F}^{\frac{1}{2}}(\boldsymbol{\theta})G_\beta(\boldsymbol{\theta}), \quad (22)$$

followed by taking square on both sides

$$\Delta\boldsymbol{\theta}^\top \mathcal{F}(\boldsymbol{\theta})\Delta\boldsymbol{\theta} = \alpha_1^2 G_\beta(\boldsymbol{\theta})^\top \mathcal{F}(\boldsymbol{\theta})\nabla G_\beta(\boldsymbol{\theta}), \quad (23)$$

where we used  $|\mathcal{F}^{\frac{1}{2}}\boldsymbol{\mu}|^2 = \boldsymbol{\mu}^\top \mathcal{F}\boldsymbol{\mu}$ . We insert Eq. (20) and get

$$\alpha_1 = \frac{2\sqrt{-\log(K_t(\boldsymbol{\theta}))}}{\sqrt{G_\beta(\boldsymbol{\theta})^\top \mathcal{F}(\boldsymbol{\theta})G_\beta(\boldsymbol{\theta})}}, \quad (24)$$

with the first update rule

$$\boldsymbol{\theta}_1 = \boldsymbol{\theta} + \alpha_1 G_\beta(\boldsymbol{\theta}). \quad (25)$$

We assumed for above calculations that the PQC is able to represent the target quantum state perfectly, i.e.  $\max_{\boldsymbol{\theta}} |\langle \psi(\boldsymbol{\theta}) | \psi_t \rangle|^2 = 1$ . If this is not the case, we have to adjust the learning rate to take this into account.

Assume the target state is given by

$$|\psi_t\rangle = \sqrt{K_0}|\psi(\boldsymbol{\theta}_t)\rangle + \sqrt{1-K_0}|\psi_o\rangle, \quad (26)$$

where  $|\psi_o\rangle$  is some state that is orthogonal to any other state that can be represented by the PQC, i.e.  $|\langle \psi_o | \psi(\boldsymbol{\theta}) \rangle|^2 = 0 \forall \boldsymbol{\theta}$  and  $K_0$  is the maximal possible fidelity of the PQC. Then, the first update rule is moving in the correct direction, however overshoots the target parameters. We now calculate the update rule that takes this into account. We find

$$K_t(\boldsymbol{\theta}) = K_0 e^{-\frac{1}{4}\Delta\boldsymbol{\theta}^\top \mathcal{F}(\boldsymbol{\theta})\Delta\boldsymbol{\theta}} \quad (27)$$

$$K_t(\boldsymbol{\theta}_1) = K_0 e^{-\frac{1}{4}(\boldsymbol{\theta}_1 - \boldsymbol{\theta}_t)^\top \mathcal{F}(\boldsymbol{\theta})(\boldsymbol{\theta}_1 - \boldsymbol{\theta}_t)} \quad (28)$$

where  $K_t(\boldsymbol{\theta}_1)$  is the fidelity after applying the first update rule. Now our goal is to find the corrected update rule

$$\boldsymbol{\theta}_t = \boldsymbol{\theta} + \alpha_t G_\beta(\boldsymbol{\theta}), \quad (29)$$

with updated learning rate  $\alpha_t$ . By subtracting the two update rules we get

$$\boldsymbol{\theta}_1 - \boldsymbol{\theta}_t = (\alpha_1 - \alpha_t)G_\beta(\boldsymbol{\theta}). \quad (30)$$

We insert above equations into the fidelities and get

$$K_t(\boldsymbol{\theta}) = K_0 e^{-\frac{1}{4}\alpha_t^2 G_\beta^\top \mathcal{F} G_\beta} \quad (31)$$

$$K_t(\boldsymbol{\theta}_1) = K_0 e^{-\frac{1}{4}(\alpha_1 - \alpha_t)^2 G_\beta^\top \mathcal{F} G_\beta} \quad (32)$$

By dividing above equations, we can solve for  $\alpha_t$  and find

$$\alpha_t = \frac{1}{2} \left( \frac{4}{\alpha_1 G_\beta(\boldsymbol{\theta})^T \mathcal{F}(\boldsymbol{\theta}) G_\beta(\boldsymbol{\theta})} \log \left( \frac{K_t(\boldsymbol{\theta}_1)}{K_t(\boldsymbol{\theta})} \right) + \alpha_1 \right) \quad (33)$$

with final update rule

$$\boldsymbol{\theta}'_t = \boldsymbol{\theta} + \alpha_t G_\beta(\boldsymbol{\theta}) \quad (34)$$

where  $\boldsymbol{\theta}'_t$  is the parameter for the PQC after one step of gradient ascent.

### Variance of gradient

We now show how to calculate the variance of the gradient  $\nabla K_t(\boldsymbol{\theta})$  using Eq. (4). We assume a PQC with  $M$  parameters, QFIM  $\mathcal{F}(\boldsymbol{\theta})$  and a target state  $|\psi_t\rangle = \sqrt{K_0}|\psi(\boldsymbol{\theta}_t)\rangle + \sqrt{1-K_0}|\psi_0\rangle$ , where  $|\psi_0\rangle$  is some state that is orthogonal to any other state that can be represented by the PQC, i.e.  $|\langle\psi_0|\psi(\boldsymbol{\theta})\rangle|^2 = 0 \forall \boldsymbol{\theta}$ . The initial state of the PQC is  $|\psi(\boldsymbol{\theta})\rangle$  with random parameter  $\boldsymbol{\theta}$ . We define the vector to the correct solution as  $\Delta\boldsymbol{\theta} = \boldsymbol{\theta}_t - \boldsymbol{\theta}$ . We now assume that the entries of the vector  $\Delta\boldsymbol{\theta}$  are sampled from the uniform distribution  $\Delta\boldsymbol{\theta}^{(n)} \sim \text{uniform}(-\sqrt{3}\frac{\sqrt{-4\log(A_0)}}{\sqrt{\text{Tr}(\mathcal{F})}}, \sqrt{3}\frac{\sqrt{-4\log(A_0)}}{\sqrt{\text{Tr}(\mathcal{F})}})$ , where  $A_0$  is identified later on. The mean is  $\langle\Delta\boldsymbol{\theta}^{(n)}\rangle = 0$  and variance  $\langle(\Delta\boldsymbol{\theta}^{(n)})^2\rangle = \frac{-4\log(A_0)}{\text{Tr}(\mathcal{F})}$ . Further, the average of the product of index  $n$  and  $m$  is given by  $\langle(\Delta\boldsymbol{\theta}^{(n)}\Delta\boldsymbol{\theta}^{(m)})\rangle = \delta_{nm}\frac{-4\log(A_0)}{\text{Tr}(\mathcal{F})}$ , where  $\delta_{nm}$  is the Kronecker delta. First, we calculate

$$\begin{aligned} \langle\Delta\boldsymbol{\theta}^T \mathcal{F} \Delta\boldsymbol{\theta}\rangle &= \sum_{n,m} \mathcal{F}_{nm} \langle\Delta\boldsymbol{\theta}^{(n)} \Delta\boldsymbol{\theta}^{(m)}\rangle \\ &= \sum_n \mathcal{F}_{nn} \langle\Delta\boldsymbol{\theta}^{(n)} \Delta\boldsymbol{\theta}^{(n)}\rangle = -4\log(A_0) \end{aligned}$$

Now, we assume that  $M$  is large, such that we can apply the central limit theorem  $\langle e^{-\frac{1}{4}\Delta\boldsymbol{\theta}^T \mathcal{F} \Delta\boldsymbol{\theta}} \rangle \approx e^{-\frac{1}{4}\langle\Delta\boldsymbol{\theta}^T \mathcal{F} \Delta\boldsymbol{\theta}\rangle}$ . Then, we find

$$A_0 = e^{-\frac{1}{4}\langle\Delta\boldsymbol{\theta}^T \mathcal{F} \Delta\boldsymbol{\theta}\rangle}. \quad (35)$$

We can now identify with the fidelity

$$K_t(\boldsymbol{\theta}) = K_0 e^{-\frac{1}{4}\langle\Delta\boldsymbol{\theta}^T \mathcal{F} \Delta\boldsymbol{\theta}\rangle} = A_0 K_0. \quad (36)$$

The gradient of the fidelity is given by

$$\nabla K_t(\boldsymbol{\theta}) = -\frac{1}{2} \mathcal{F} \Delta\boldsymbol{\theta} K_0 e^{-\frac{1}{4}\langle\Delta\boldsymbol{\theta}^T \mathcal{F} \Delta\boldsymbol{\theta}\rangle}. \quad (37)$$

We now want to calculate the variance of the  $n$ -th element of the gradient vector. The mean of the gradient  $\langle\nabla K_t(\boldsymbol{\theta})\rangle = 0$ . For the square of the gradient, we find

$$\langle(\nabla K_t(\boldsymbol{\theta})^{(n)})^2\rangle = \frac{1}{4} \langle((\mathcal{F} \Delta\boldsymbol{\theta})^{(n)})^2\rangle K_0^2 e^{-\frac{1}{8}\langle\Delta\boldsymbol{\theta}^T \mathcal{F} \Delta\boldsymbol{\theta}\rangle}. \quad (38)$$

We now calculate the element

$$\begin{aligned} \langle((\mathcal{F} \Delta\boldsymbol{\theta})^{(n)})^2\rangle &= \sum_{k,m} \langle\mathcal{F}_{nm} \Delta\boldsymbol{\theta}^{(m)} \mathcal{F}_{nk} \Delta\boldsymbol{\theta}^{(k)}\rangle \\ &= \sum_m \mathcal{F}_{nm} \mathcal{F}_{nm} \langle(\Delta\boldsymbol{\theta}^{(m)})^2\rangle = \sum_m \mathcal{F}_{nm} \mathcal{F}_{mn} \frac{-4\log(A_0)}{\text{Tr}(\mathcal{F})} \\ &= \frac{-4\log(A_0) (\mathcal{F}^2)_{nn}}{\text{Tr}(\mathcal{F})} \end{aligned}$$

where we used  $\mathcal{F}_{mn} = \mathcal{F}_{nm}$  and  $\sum_m \mathcal{F}_{nm} \mathcal{F}_{nm} = \sum_m \mathcal{F}_{nm} \mathcal{F}_{mn} = (\mathcal{F}^2)_{nn}$ . Now, we take the average over the variance of the different gradient entries  $n$  and use the Pythagorean theorem (i.e. one can sum over the variance of independent variables)

$$\begin{aligned} \langle\langle(\mathcal{F} \Delta\boldsymbol{\theta})^{(n)}\rangle\rangle_{\Delta\boldsymbol{\theta}} &= \frac{1}{M} \sum_n \langle\langle(\mathcal{F} \Delta\boldsymbol{\theta})^{(n)}\rangle\rangle \\ &= \frac{-4\log(A_0) \text{Tr}(\mathcal{F}^2)}{M \text{Tr}(\mathcal{F})}, \end{aligned}$$

where  $\langle\langle.\rangle\rangle_{\Delta\boldsymbol{\theta}}$  indicates that we average first over  $\Delta\boldsymbol{\theta}^{(n)}$  and then  $n$ . Finally, we get

$$\begin{aligned} \langle\langle(\nabla K_t(\Delta\boldsymbol{\theta})^{(n)})^2\rangle\rangle_{\Delta\boldsymbol{\theta}} &= -\log \left[ \frac{K_t(\boldsymbol{\theta})}{K_0} \right] \frac{\text{Tr}(\mathcal{F}^2)}{M \text{Tr}(\mathcal{F})} K_0^2 e^{-\frac{1}{8}\langle\Delta\boldsymbol{\theta}^T \mathcal{F} \Delta\boldsymbol{\theta}\rangle} \\ &= \log \left[ \frac{K_0}{K_t(\boldsymbol{\theta})} \right] K_t(\boldsymbol{\theta})^2 \frac{\text{Tr}(\mathcal{F}^2)}{M \text{Tr}(\mathcal{F})}. \end{aligned} \quad (39)$$

The variance becomes maximal when  $K_t(\boldsymbol{\theta}) = K_0 \exp(-\frac{1}{2}) \approx 0.6K_0$ . The variance of the gradient decays linearly with number of parameters  $M$  and is independent of qubit number  $N$ .

We now derive the lower bound of the variance. The variance of the eigenvalues of  $\mathcal{F}$  with  $M$  eigenvalues  $\lambda_n$  is always greater zero

$$\begin{aligned} \frac{1}{M} \sum_{n=1}^M \lambda_n^2 - \left( \frac{1}{M} \sum_{n=1}^M \lambda_n \right)^2 &\geq 0 \\ \sum_{n=1}^M \lambda_n^2 &\geq \frac{1}{M} \left( \sum_{n=1}^M \lambda_n \right)^2. \end{aligned}$$

With the relation  $\text{Tr}(\mathcal{F}) = \sum_{n=1}^M \lambda_n$  and  $\text{Tr}(\mathcal{F}^2) = \sum_{n=1}^M \lambda_n^2$ , we find

$$\text{Tr}(\mathcal{F}^2) \geq \frac{1}{M} \text{Tr}(\mathcal{F})^2. \quad (40)$$

Thus, the variance is lower bounded by

$$\text{var}(\partial_k K_t(\boldsymbol{\theta})) \geq \frac{\text{Tr}(\mathcal{F}(\boldsymbol{\theta}))}{M^2} K_t(\boldsymbol{\theta})^2 \log \left[ \frac{K_0}{K_t(\boldsymbol{\theta})} \right]. \quad (41)$$

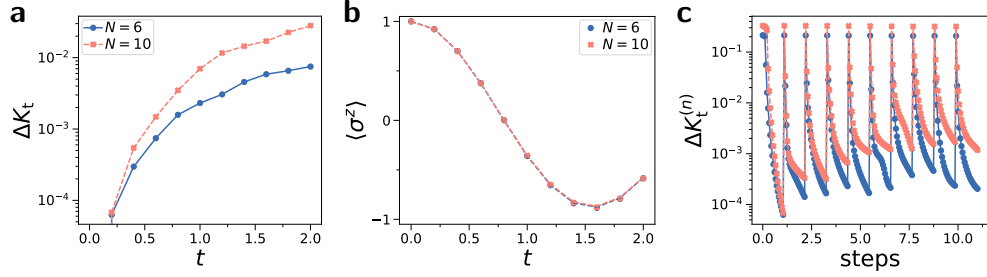


FIG. 15. Demonstration of projected variational quantum dynamics using adaptive gradient descent with GQNG. **a)** Fidelity in respect to the exact solution. **b)** Magnetization found compared to exact solution in dashed lines **c)** training loss for each Trotter step  $N_s$ , each trained with  $N_t$  training iterations. We simulate the evolution for total time  $T = N_s \Delta t$  using  $N_s = 10$  Trotter steps and  $\Delta t = 0.2$ , with each step trained with  $N_t = 20$  training steps. The PQC used is YZ-CNOT with  $p = N$ ,  $J = 0.25$ ,  $h = 1$  and initial state is the computational basis state with all zeros.

### Fidelity of time evolution

Here, we show the fidelity of a time evolved state. Assume we evolve the state  $|\psi\rangle$  with the Hamiltonian  $H$  for a time  $\Delta t$ . The eigenstates of  $H$  are given by  $|\phi_n\rangle$  and eigenenergies by  $\lambda_n$ . The initial state is now expressed in terms of the eigenstates  $|\psi\rangle = \sum_n \beta_n |\phi_n\rangle$ , with overlap  $\beta_n$  with the  $n$ -th eigenstate. We assume that  $|\psi\rangle$  has only non-zero overlap  $\beta_n \neq 0$  with  $L$  eigenstates, where  $\lambda_1$  is the smallest and  $\lambda_L$  the largest eigenvalue with non-zero overlap. We define  $\Delta E = \lambda_L - \lambda_1$ . Now, the evolved state is given by  $|\psi'\rangle = \exp(-iH\Delta t)|\psi\rangle = \sum_{n=1}^L \beta_n e^{-i\lambda_n \Delta t} |\phi_n\rangle$ . The fidelity between initial and evolved state is given by

$$K = |\langle \psi' | \psi \rangle|^2 = \left| \sum_{n=1}^L \beta_n^2 e^{-i\lambda_n \Delta t} \right|^2 = \quad (42)$$

We now derive a lower bound for  $K$  for small times  $\Delta t$ .  $K$  is minimal for small  $\Delta t$  when  $|\beta_1|^2 = \frac{1}{2}$  and  $|\beta_L|^2 = \frac{1}{2}$ . This is evident as the relative phase between largest and smallest eigenvalues evolves the fastest. We have in this case

$$K = \frac{1}{2} (1 + \cos((\lambda_L - \lambda_1) \Delta t)) = \cos^2\left(\frac{\Delta E \Delta t}{2}\right). \quad (43)$$

Now, a lower bound for  $K$  can be found via a first order Taylor expansion

$$K > 1 - \frac{1}{4} (\Delta E \Delta t)^2. \quad (44)$$

### Projected variational quantum dynamics

Here, we simulate the dynamics of the transverse Ising model with the projected variational quantum dynamics method [24]. The Hamiltonian is given by

$$H = J \sum_{n=1}^N \sigma_n^z \sigma_{n+1}^z + h \sum_{i=1}^N \sigma_n^x \quad (45)$$

In Fig.15a, we show the fidelity in respect to the exact solution. In Fig.15b, we show the dynamics of the  $\langle \frac{1}{N} \sum_i \sigma_i^z \rangle$  over time  $t$ . We observe good match between simulation and exact result. In Fig.15c, we show the training loss for each of the Trotter steps.